Journal of Power Sources 203 (2012) 177–183

Contents lists available at SciVerse ScienceDirect

Journal of Power Sources

journal homepage: www.elsevier.com/locate/jpowsour

Synthesis and electrochemical performance of mixed phase α/β nickel hydroxide

Yanwei Li[a,b,*], Jinhuan Yao[a], Yanxi Zhu[a], Zhengguang Zou[b], Hongbo Wang[c]

[a] GuangXi Key Laboratory of New Energy and Building Energy Saving, College of Chemistry and Bioengineering, Guilin University of Technology, Guilin 541004, PR China
[b] Key Laboratory of New Processing Technology for Nonferrous Metals and Materials, Ministry of Education, Guilin University of Technology, Guilin 541004, PR China
[c] School of Chemistry and Chemical Engineering, Nanjing University, Nanjing 210008, PR China

ARTICLE INFO

Article history:
Received 16 August 2011
Received in revised form
27 November 2011
Accepted 30 November 2011
Available online 8 December 2011

Keywords:
Nickel hydroxide
Electrode material
Mixed phase
Secondary batteries
Microstructure
Electrochemical performance

ABSTRACT

Nickel hydroxide with a unique α/β mixed phase structure is synthesized by partially substituting Al^{3+} for Ni^{2+} with chemical coprecipitation method. The physical properties of the synthesized Al-substituted α/β-nickel hydroxide are characterized by X-ray diffraction (XRD), Fourier transform infrared spectroscopy (FT-IR), thermogravimetry analysis (TG), scanning electron microscopy (SEM), inductively coupled plasma atomic emission spectroscopy (ICP-AES), and tap density testing. The results show that the Al-substituted α/β-nickel hydroxide exhibits an irregular shape and contains many intercalated water molecules. In particular, the tap density of the Al-substituted α/β-nickel hydroxide reaches 2.02 g cm^{-3}, which is significantly higher than that of α-nickel hydroxide. The electrochemical performances of the prepared samples are characterized by cyclic voltammetry (CV), electrochemical impedance spectroscopy (EIS), and charge/discharge tests. The results demonstrate that the Al-substituted α/β-nickel hydroxide has much higher electrochemical activity, better electrochemical reversibility, lower electrochemical reaction impedance, and higher discharge voltage than the pure β-nickel hydroxide. The specific discharge capacity of the Al-substituted α/β-nickel hydroxide maintains to be 325.4 mAh g^{-1} (or 657.3 mA h cm^{-3}) after 100 cycles at a charging/discharging current density of 200 mA g^{-1} under ambient temperature.

1. Introduction

Nickel hydroxide compounds are widely used as the active material of positive electrode in alkaline secondary batteries (nickel–metal hydride (Ni–MH), nickel–zinc (Ni–Zn), nickel–iron (Ni–Fe), and nickel–cadmium (Ni–Cd) batteries) [1]. Typically, nickel hydroxide has two polymorphic forms known as α-$Ni(OH)_2$ and β-$Ni(OH)_2$, which in the oxidation process transform into γ-NiOOH and β-NiOOH, respectively [2]. In commercial batteries, β-$Ni(OH)_2$ is usually used because it has a high tap density and good stability in strong alkaline electrolyte [3–7]. However, the theoretical capacity of β-$Ni(OH)_2$ is only 289 mA h g^{-1} due to the one-electron-exchange reaction in β-$Ni(OH)_2$/β-NiOOH couple. This theoretical capacity has been approximately reached in current commercial alkaline secondary batteries. Moreover, if overcharge happens, the β-NiOOH transforms partially into γ-NiOOH, which results in a large volume expansion of the electrode and causes rapid capacity decay during electrochemical charge/discharge cycles [8].

The α-$Ni(OH)_2$ is capable of realizing a two-electron-exchange reaction through the electrochemical conversion between α-$Ni(OH)_2$/γ-NiOOH couple. The average oxidation state of nickel in γ-NiOOH is 3.3–3.7 [9]. Therefore, a much higher discharge capacity can be obtained for α-$Ni(OH)_2$. In addition, α-$Ni(OH)_2$ exhibits no noticeable volume change when repeatedly charge/discharge cycled between α-$Ni(OH)_2$/γ-NiOOH couple because of the similar lattice of α-$Ni(OH)_2$ and γ-NiOOH. However, pure α-$Ni(OH)_2$ is very unstable in a strong alkaline electrolyte and easily transforms to β-$Ni(OH)_2$. In order to improve the stability of α-$Ni(OH)_2$ in strong alkaline electrolyte, many efforts have been focused on the preparation of stabilized α-$Ni(OH)_2$ by partial substitution of Ni ion in the nickel hydroxide lattice by other metal ions, such as Al [10], Co [11], Fe [12], Mn [13], and Zn [14] ions. Among these metal ions, Al ion is the most attractive because of its high stability at trivalent state and cheapness. It should be noted that the substitution approach has a side effect that the discharge capacity usually decreases with the increasing amount of substituting Al ion because Al ion is an electrochemically inert element during the electrochemical redox reaction. Therefore, the amount of substituting Al ion in α-$Ni(OH)_2$ should be kept as low as possible.

* Corresponding author at: GuangXi Key Laboratory of New Energy and Building Energy Saving, College of Chemistry and Bioengineering, Guilin University of Technology, Guilin 541004, PR China. Tel.: +86 773 5896446; fax: +86 773 5896671.
E-mail address: lywhit@glite.edu.cn (Y. Li).

0378-7753/$ – see front matter © 2011 Elsevier B.V. All rights reserved.
doi:10.1016/j.jpowsour.2011.11.081

The Al ion substitution not only changes the chemical composition but also influences the phase composition of nickel hydroxide product and accordingly affects the electrode properties [15]. Usually, a mixture nickel hydroxide product with α-phase and β-phase can be obtained by carefully controlling the amount of Al ion substitution. Although there are numerous papers on Al-substituted α-nickel hydroxide, few papers are found to study the structure and electrochemical performance of the Al-substituted nickel hydroxide with unique α/β mixed phase structure. Tu et al. [16] added different amount of nanosized α-$Ni(OH)_2$ into the microscale β-$Ni(OH)_2$ and investigated the electrochemical properties of this biphase nickel hydroxide. They found that the biphase nickel hydroxide with 10 wt% nanosized α-$Ni(OH)_2$ exhibits better charge/discharge cyclic stability and higher discharge capacity than that of β-$Ni(OH)_2$ electrode. Since β-$Ni(OH)_2$ has a better structural stability and α-$Ni(OH)_2$ has a higher discharge capacity, the nickel hydroxide with α-phase and β-phase is expected to have better electrochemical performance. Based on the above consideration, the present work aims to investigate the structure and electrochemical performance of Al-substituted nickel hydroxide with α/β mixed phase structure. The Al-substituted α/β-nickel hydroxide was synthesized by a chemical coprecipitation method. The physical properties of the prepared samples were characterized by X-ray diffraction (XRD), Fourier transform infrared spectroscopy (FT-IR), thermogravimetry analysis (TG), scanning electron microscopy (SEM), inductively coupled plasma atomic emission spectroscopy (ICP-AES), and tap density testing. The electrochemical performances of the prepared sample were investigated by cyclic voltammetry (CV), electrochemical impedance spectroscopy (EIS), and charge/discharge tests.

2. Experimental

2.1. Sample preparation and characterization

The Al-substituted α/β-nickel hydroxide was prepared by chemical coprecipitation method. First, 1.0 mol L^{-1} NaOH was added dropwise into a mixture solution containing $Ni(NO_3)_2{\cdot}6H_2O$ and $Al(NO_3)_3{\cdot}9H_2O$ (in a $[Al^{3+}/Ni^{2+}]$ molar ratio of 1/10) under magnetic stirring at 60 °C. The final pH value of the mixture solution was controlled to be 10–11. After continual stirring for 3 h, the obtained suspension was kept in mother solution at 60 °C for 20 h and then collected by filtration. The precipitate was washed with deionized water to a neutral state, and dried at 60 °C in air to a constant weight. As comparison, the pure β-$Ni(OH)_2$ was also prepared under similar conditions as described above but without adding $Al(NO_3)_3{\cdot}9H_2O$ in the reaction solution.

The phase structure of the prepared samples was identified with a X-ray diffractometer (Panalytical X' Pert PRO) using Cu Kα radiation source (λ = 1.5418 Å, 40.0 kV, 100 mA). Infrared spectra of the prepared samples were obtained on a Fourier transform infrared spectrometer (FT-IR, Thermo Nicolet NEXUS 470). The surface morphology and metals content of the prepared samples were characterized by scanning electron microscopy (SEM, Hitachi S-570) equipped with energy dispersive spectroscopy (EDS). The metals content of Al-substituted α/β-nickel hydroxide was also analyzed using inductively coupled plasma atomic emission spectroscopy (ICP-AES, IRIS Advantage). A JZ-1 tap density tester (China) was used to determine the tap density of the prepared samples. Thermal gravity analysis (TG) of the prepared samples was carried out with a thermal analyzer (Netzsch STA 449C) heating from 50 °C to 800 °C at a heating rate of 10 °C min^{-1}.

2.2. Preparation of nickel electrode

The pasted nickel electrodes were prepared as follows: the prepared nickel hydroxide sample, nickel powder, graphite, and acetylene black were mixed thoroughly in a weight ratio of 85/5/5/5. A proper amount of polytetrafluoroethylene (PTFE, 5 wt%) binder was added to the above mixture to obtain homogenous slurry with adequate rheological properties. The slurry was filled into a nickel foam sheet. The obtained nickel electrodes were dried at 60 °C and then pressed under a pressure of 8 MPa for 5 min to assure good electrical contact between nickel foam and active material. The nickel electrodes were first soaked in 6.0 mol L^{-1} KOH electrolyte for 24 h to assure complete penetration of electrolyte into the nickel electrodes prior to electrochemical measurements.

2.3. Electrochemical measurement

Cyclic voltammetry (CV) and electrochemical impedance spectroscopy (EIS) measurements were carried out using an Autolab PGSTAT12 Electrochemical Workstation (ECO Chemie BV, Utrecht, Netherlands) in a classical three-compartment electrolysis cell at ambient temperature. The prepared nickel electrode was used as working electrode. The counter electrode was a piece of nickel foam sheet and the reference electrode was an Hg/HgO electrode. A 6.0 mol L^{-1} KOH aqueous solution was used as electrolyte. The scan rate for CV measurement was 0.1 mV s^{-1} and the cell potential ranged from 0.0 V to 0.8 V *vs.* Hg/HgO. EIS measurement was made at open circuit potential with a superimposed 5 mV sinusoidal voltage in the frequency range from 10 kHz to 10 mHz.

Galvanostatic charge/discharge measurement of nickel electrodes was conducted using a Land Battery Testing Equipment (CT2001C) at ambient temperature. Test cells were assembled using the prepared nickel electrode as the cathode, a commercial hydrogen-storage alloy electrode as the anode, and polypropylene as the separator. A 6.0 mol L^{-1} KOH aqueous solution was used as electrolyte. The nickel electrodes were charged at a current density of 50 mA g^{-1}, and then discharged to 1.0 V with the same current density for activation. Such four cycles were done before further charge/discharge measurements at the constant current density of 200 mA g^{-1}. The current densities and discharge capacities in this work were all calculated according to the actual mass of the synthesized nickel hydroxide samples used in the nickel electrode preparation.

3. Results and discussion

3.1. Physical properties of the prepared nickel hydroxide

Fig. 1 gives the XRD patterns of the prepared nickel hydroxide samples. For comparison, the positions of standard diffraction peaks of α-$Ni(OH)_2{\cdot}0.75H_2O$ (JCPDS 38-715) and β-$Ni(OH)_2$ (JCPDS 14-117) are also given at the bottom in Fig. 1. For the nickel hydroxide without Al, all the diffraction peaks can be indexed as pure β-$Ni(OH)_2$. The lattice parameters a (=$2d_{1\,1\,0}$) and c (=$d_{0\,0\,1}$) of this pure β-$Ni(OH)_2$ evaluated from Bragg formula are 3.125 Å and 4.591 Å, respectively. For the Al-substituted nickel hydroxide, the diffraction peaks from both α-$Ni(OH)_2$ and β-$Ni(OH)_2$ are detected, indicating that it is a two-phase mixture. The lattice parameter a (=$2d_{1\,1\,0}$) of the Al-substituted α-nickel hydroxide in the two-phase mixture evaluated from Bragg formula is 3.066 Å, which is smaller than that (3.125 Å) of the pure β-$Ni(OH)_2$. This is caused by the smaller ionic radius of Al (0.54 Å) compared to Ni (0.69 Å) in the lattice of nickel hydroxide [15,17]. The lattice parameter c (=$3d_{0\,0\,3}$) of the rhombohedral Al-substituted α-nickel hydroxide in the two-phase mixture evaluated from Bragg formula is

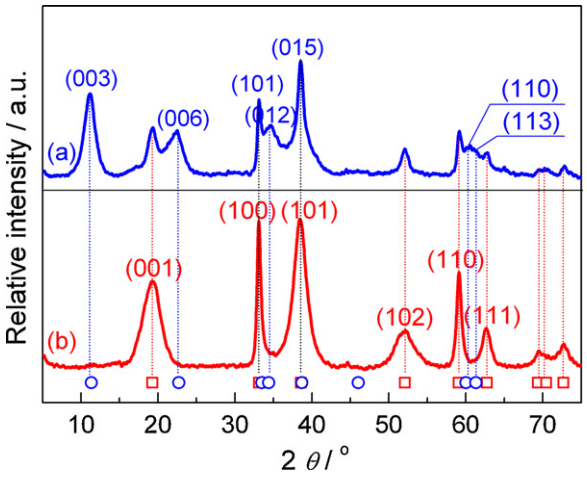

Fig. 1. XRD patterns of: (a) Al-substituted α/β-nickel hydroxide and (b) pure β-$Ni(OH)_2$. The lines of open circles and squares at the bottom represent the position of the standard XRD peaks of α-$Ni(OH)_2$ and β-$Ni(OH)_2$, respectively.

23.82 Å. The interlayer spacing (d_{003} = 7.94 Å) of the Al-substituted α-nickel hydroxide in the two-phase mixture is larger than that (7.27 Å–7.32 Å) of pure α-$Ni(OH)_2$ [18,19]. This increased interlayer spacing is probably caused by an increase in the intercalated anions in the Al-substituted α-nickel hydroxide lattice, which are necessary for compensating the charge excess due to Al^{3+}. The interlayer spacing of the β-nickel hydroxide in the two-phase mixture evaluated from Bragg formula is 4.591 Å, which is identical with that (4.591) of the pure β-$Ni(OH)_2$. The identical interlayer spacing indicates that Al^{3+} may not substitute Ni^{2+} in the β-nickel hydroxide of two-phase mixture.

To complement the XRD measurements, FT-IR spectra for the prepared nickel hydroxide samples were made and the results are shown in Fig. 2. The pure β-$Ni(OH)_2$ presents characteristic bands for nitrate ion, hydroxyl groups, and adsorbed water molecules. The sharp band at about 3640 cm^{-1} and the broad band at about 3420 cm^{-1} correspond to stretching vibrations of hydroxyl groups in the nickel hydroxide lattice and the adsorbed water, respectively [20]. The two weak bands at about 1620 cm^{-1} and 1390 cm^{-1} are due to the angular deformation of adsorbed water molecule and stretching vibrations of adsorbed anions (nitrate ions and carbonate ions), respectively [11,18,21]. At low wavenumbers, the couple bands at about 523 cm^{-1} and 465 cm^{-1} are associated with Ni—O—H

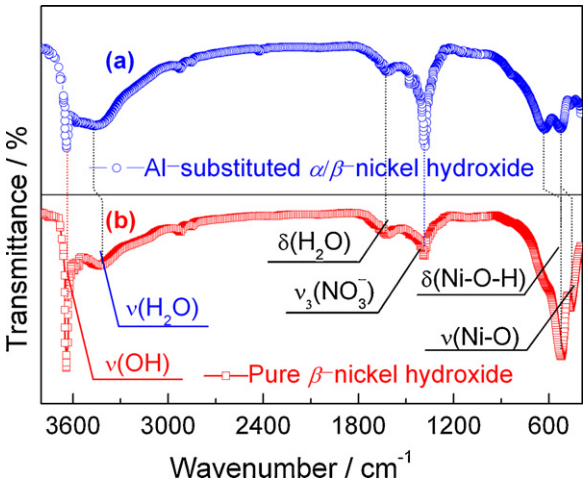

Fig. 2. FT-IR spectra of: (a) Al-substituted α/β-nickel hydroxide and (b) pure β-$Ni(OH)_2$.

bending and Ni—O stretching vibrations, respectively [22,23]. In addition to these adsorptions, the FT-IR spectrum of Al-substituted α/β-nickel hydroxide shows peak due to stretching vibration of hydroxyl group of intercalated and adsorbed water molecules at about 3450 cm^{-1}. The intense band at 1390 cm^{-1} for Al-substituted α/β-nickel hydroxide is assigned to intercalated anions (nitrate ions and carbonate ions). The presence of carbonate ions is due to the open system used in the synthesis. Contrast to the small interlayer spacing (4.591 Å) of pure β-$Ni(OH)_2$, the Al-substituted α-nickel hydroxide in the two-phase mixture has a larger interlayer spacing of 7.94 Å that can host variable amounts of water molecules and anionic species. The orderly arrangement of these intercalated anions resulted from the hydrogen-bond action causes the sharp absorption peak [24]. The intercalated anions play an important role in maintaining the α-type phase structure through electrostatic attractions between positively charged hydroxide slabs and negative charged anionic species. The bend vibration of M—O—H and the stretching vibration of M—O of Al-substituted α/β-nickel hydroxide are blue shifted, which are characteristic of α-nickel hydroxide motifs [25,26].

Fig. 3 presents the SEM photographs of Al-substituted α/β-nickel hydroxide and pure β-$Ni(OH)_2$. It can be seen that both samples appear to be aggregates of irregular shapes, very similar to the Al-substituted α-nickel hydroxide powders prepared by homogenous precipitation method [27] and electrochemical impregnation method [28]. In addition, the Al-substituted α/β-nickel hydroxide particles seem more dense than the pure β-$Ni(OH)_2$. Generally, nickel hydroxide powders with irregular shape possess a higher specific surface area which can provide a high density of active sites and accordingly promote intimate interaction between the active material and the surrounding electrolyte [29,30]. The tap density of the pure β-$Ni(OH)_2$ prepared in this work is 1.65 g cm^{-3}, which is very similar with the tap density (1.62 g cm^{-3}) of the chemical precipitated non-spherical nickel hydroxides prepared by Chang et al. [31]. The tap density of the Al-substituted α/β-nickel hydroxide is 2.02 g cm^{-3}. This value is slightly lower than that (2.1–2.2 g cm^{-3}) of commercial spherical nickel hydroxide but much higher than that (<1.7 g cm^{-3}) of α-nickel hydroxide [32]. The high tap density of the Al-substituted α/β-nickel hydroxide may originate from the different *K*sp of $Al(OH)_3$ (1.3×10^{-33}) and $Ni(OH)_2$ (5.5×10^{-16}). Since the *K*sp of $Al(OH)_3$ is much smaller than that of $Ni(OH)_2$, the deposition of Al^{3+} in the $Ni(OH)_2$ lattice may be quicker than that of Ni^{2+}, which may provide a net structure and facilitate the agglomerations of colloidal nickel hydroxide particles. The agglomerations squeeze out water and further increase the structure's density. Due to this dense structure, the Al-substituted α/β-nickel hydroxide particles are prone to grow and crystallize in the subsequent drying process, and therefore the tap density remarkably increases.

Fig. 4 gives the EDS spectrum of the Al-substituted α/β-nickel hydroxide sample. It can be seen that Al is successfully doped in the lattice of nickel hydroxide. The molar ratio of [Al^{3+}/Ni^{2+}] on the surface of Al-substituted α/β-nickel hydroxide coming from EDS result is 0.96/10, which is slightly lower than that (1.06/10) from ICP-AES result. The amount of water molecules intercalated in nickel hydroxide plays an important role in the crystal structure and electrochemical properties. In this work, TG analysis has been used to investigate the water content and the dehydration reaction of nickel hydroxide. Fig. 5 shows the TG curves of Al-substituted α/β-nickel hydroxide and pure β-$Ni(OH)_2$. The TG curve of pure β-$Ni(OH)_2$ shows two obvious weight loss regions. The first region below 185 °C with a weight loss of about 5.7% is due to the loss of adsorbed water molecules. The second region between 185 °C and 450 °C with a weight loss of about 19.2% is due to the decomposition of nickel hydroxide into NiO, H_2O, and the loss of adsorbed anions of the mother solution [33]. The TG curve of Al-substituted α/β-nickel

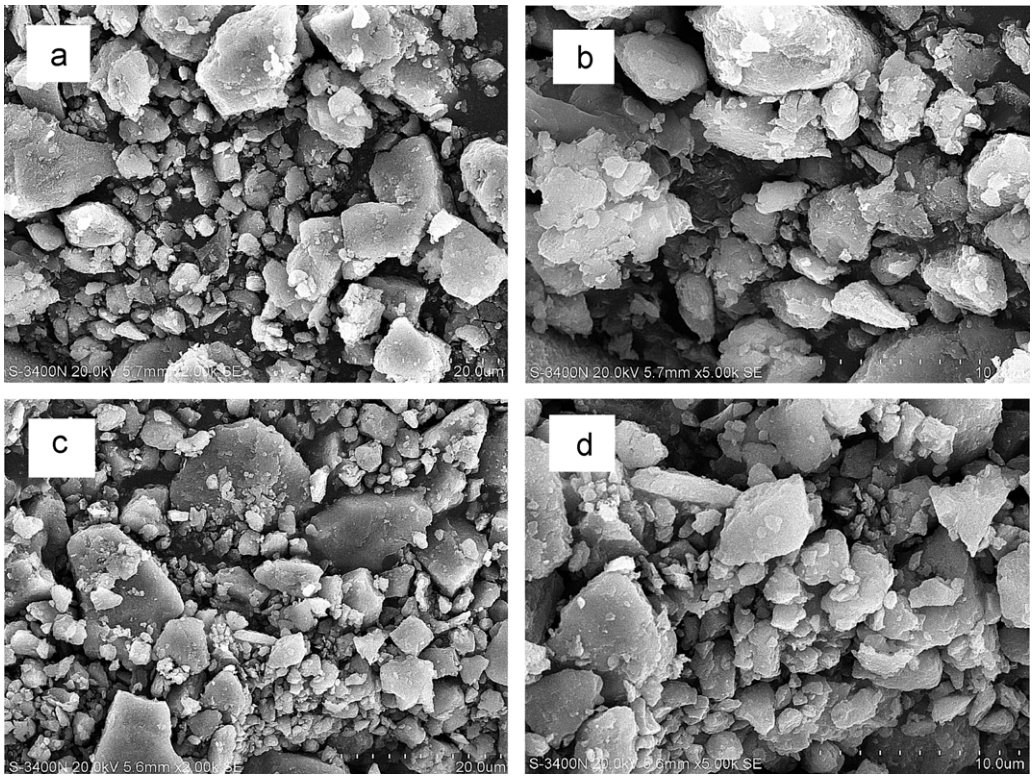

Fig. 3. SEM images of: (a and b) pure β-Ni(OH)$_2$ and (c and d) Al-substituted α/β-nickel hydroxide.

hydroxide shows three weight loss regions. The first region below 75 °C with a weight loss of about 3.3% is due to the loss of adsorbed water molecules. The second region between 75 °C and 185 °C with a weight loss of about 5.9% is mainly attributed to the loss of water molecules that structurally bonded in between the nickel hydroxide lattices [18]. These structurally bonded water (intercalated water) molecules provide the passage for proton diffusion along the molecular chain between layers, which may accelerate the proton diffusion rate. The total water content of Al-substituted α/β-nickel hydroxide is about 9.2 wt%, which is much higher than that (5.7 wt%) of pure β-Ni(OH)$_2$. The third region between 185 °C and 450 °C with a weight loss of about 22.0% is due to Al-substituted α/β-nickel hydroxide being decomposed into NiO, Al_2O_3, H_2O, and the loss of adsorbed and intercalated anions (nitrate ions and carbonate ions) [34,35]. Based on the results of XRD, ICP-AES, FT-IR, and TG analysis, the chemical composition for Al-substituted α/β-nickel hydroxide can be expressed as follows:

$$\alpha/\beta\text{-}[Ni_{0.904}Al_{0.096}(OH)_2]^{0.096+}\cdot[M_x{}^{-}D_y{}^{2-}]^{0.096-}\cdot 0.594H_2O,$$

where M and D are mono anions (NO_3^- and OH^-) and divalent (CO_3^{2-}) anions, and $x + 2y = 0.096$.

3.2. CV and EIS measurements of the prepared nickel hydroxide

Fig. 6 shows the stable CV curves of Al-substituted α/β-nickel hydroxide and pure β-Ni(OH)$_2$ electrodes at a scan rate of 0.1 mV s^{-1}. For pure β-Ni(OH)$_2$, the oxidation peak potential (E_O) locates at 533 mV and the reduction peak potential (E_R) locates at 267 mV. For Al-substituted α/β-nickel hydroxide, both the E_O and E_R shift to more positive positions at 547 mV and 317 mV,

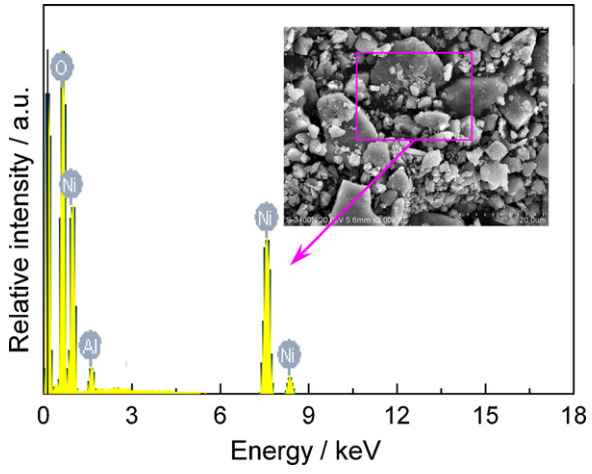

Fig. 4. EDS spectrum of Al-substituted α/β-nickel hydroxide (the selected region is illustrated in the inset SEM image).

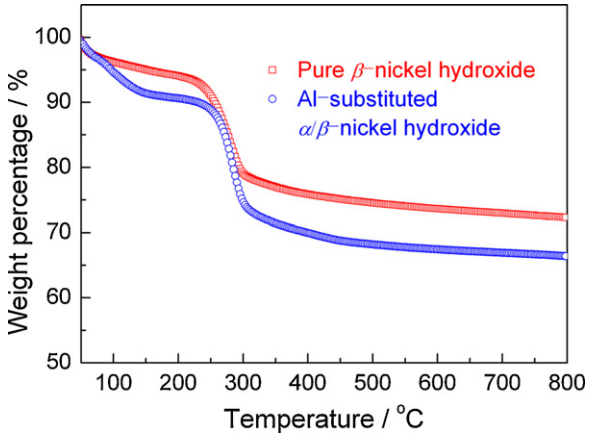

Fig. 5. TG curves of pure β-Ni(OH)$_2$ and Al-substituted α/β-nickel hydroxide.

Table 1
Electrochemical parameters from the CV curves of Al-substituted α/β-nickel hydroxide and pure β-$Ni(OH)_2$.

Material	E_R/mV	E_O/mV	E_{OE}/mV	$(E_O - E_R)$/mV	$(E_{OE} - E_O)$/mV
α/β-Nickel hydroxide	317	547	658	230	111
Pure β-$Ni(OH)_2$	267	533	608	266	75

E_R: reduction potential; E_O: oxidation potential; E_{OE}: oxygen-evolution potential.

respectively. By a detailed observation, we can find that the broad oxidation peak and reduction peak of Al-substituted α/β-nickel hydroxide are actually a superposition of the reaction peaks of both α-nickel hydroxide and β-nickel hydroxide. This result is in good agreement with the phase composition in XRD pattern. In addition, there is a couple of minor oxidation/reduction peaks located at 610 mV and 380 mV on the CV curve of pure β-$Ni(OH)_2$ sample. It is well known that trivalent β-NiOOH can be transformed into γ phase upon overcharge. Moreover, γ-NiOOH can be reduced to α-$Ni(OH)_2$. Therefore, the couple of minor oxidation/reduction peaks for pure β-$Ni(OH)_2$ sample is related to the electrochemical reaction of α-$Ni(OH)_2/\gamma$-NiOOH couples.

To compare the CV characteristics of Al-substituted α/β-nickel hydroxide and pure β-$Ni(OH)_2$ electrodes, the results of CV measurements are tabulated in Table 1. The potential difference $(E_O - E_R)$ between E_O and E_R can be used to characterize the reversibility of redox reaction [3,36]. Smaller $E_O - E_R$ means more reversible electrode reaction. The $E_O - E_R$ value of Al-substituted α/β-nickel hydroxide electrode is 230 mV, which is 36 mV smaller than that (266 mV) of pure β-$Ni(OH)_2$ electrode, suggesting that Al-substituted α/β-nickel hydroxide has better reaction reversibility. Oxygen evolution is a side reaction during the charging of nickel electrode. Oxygen evolution reaction may contribute significantly to the electrode degradation by generating internal tensile stress within the pores of the porous pasted nickel electrode and accordingly influence the cyclic performance of the electrodes and batteries [37]. Moreover, oxygen evolution reaction lowers the charging and coulombic efficiency of the electrodes during charge/discharge cycle. To compare the oxygen evolution reaction of Al-substituted α/β-nickel hydroxide electrode and pure β-$Ni(OH)_2$ electrode, the potential at 300 mA g^{-1} of anodic current density is adopted, since the return sweep can provide the best approximation of the steady-state condition with less interference from the nickel hydroxide redox reaction [38]. The results in Table 1 show that oxygen evolution potential (E_{OE}) of Al-substituted α/β-nickel hydroxide electrode shifts to a more positive value as compared with pure β-$Ni(OH)_2$ electrode. The potential difference $(E_{OE} - E_O)$ between E_{OE} and E_O of Al-substituted α/β-nickel hydroxide electrode increases obviously in comparison with

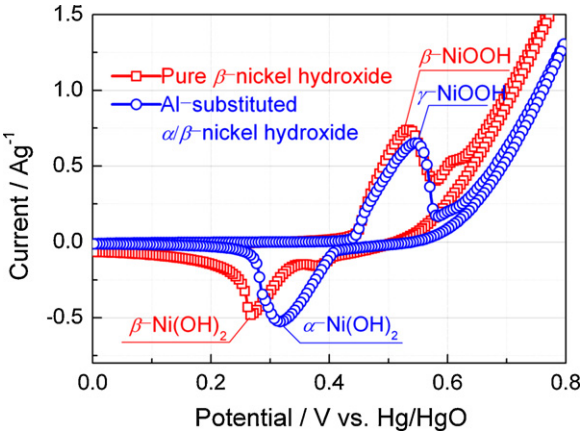

Fig. 6. Cyclic voltammograms of pure β-$Ni(OH)_2$ and Al-substituted α/β-nickel hydroxide at a scanning rate of 0.1 mV s^{-1}.

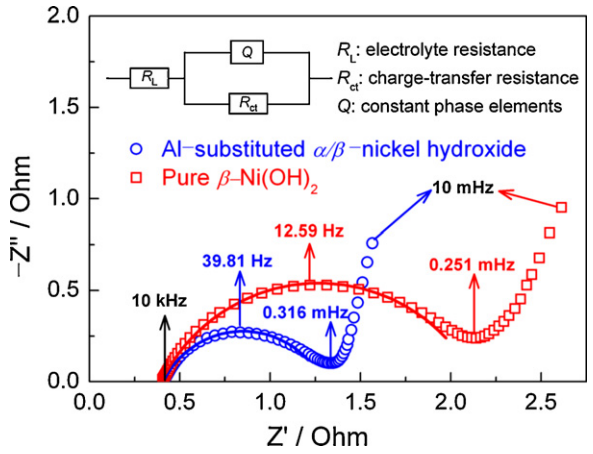

Fig. 7. Nyquist plots of pure β-$Ni(OH)_2$ and Al-substituted α/β-nickel hydroxide, where the equivalent circuit is also displayed. The symbols and solid lines correspond to the experimental data and fitting curves, respectively.

that of pure β-$Ni(OH)_2$ electrode. The large $E_{OE} - E_O$ value facilitates the electrode to be charged fully before oxygen evolution. Therefore, it can be inferred that Al-substituted α/β-nickel hydroxide electrode would exhibit much better electrochemical cycling properties than pure β-$Ni(OH)_2$ electrode.

Fig. 7 presents the Nyquist plots of Al-substituted α/β-nickel hydroxide and pure β-$Ni(OH)_2$ electrodes at steady state after being activated by cyclic voltammetric test. It can be seen that the Nyquist plots of both electrodes display a depressed semicircle resulting from charge-transfer resistance in the high frequency region [39]. To obtain the charge-transfer resistance of the two electrodes, we simulated the measured data in high frequency region by the equivalent circuit shown in Fig. 7. In the equivalent circuit, R_L and R_{ct} represent the electrolyte resistance and charge-transfer resistance, respectively; Q is the constant phase elements (CPE). $Q = Y(j\omega)^n$ where Y is the admittance, j is the imaginary unit, ω is the angular frequency, and n is the frequency power. For $n = 1$, Q is a pure capacitance and for $n = 0.5$, Q is a Warburg-type diffusion impedance. In Fig. 7, lines are the fitted results and symbols are the measured data. The best fitting results of the Nyquist curves in high frequency region from the equivalent circuit $R_L(Q{\cdot}R_{ct})$ are shown in Table 2. The charge-transfer resistance R_{ct} of pure β-$Ni(OH)_2$ electrode is 1.74 Ω, which is nearly twice as large as that (0.88 Ω) of Al-substituted α/β-nickel hydroxide electrode. This implies that the electrochemical reaction within Al-substituted α/β-nickel hydroxide proceeds more easily than that within pure β-$Ni(OH)_2$. Generally, electrochemical polarization correlates with the discharge potential. Smaller polarization means higher discharge potential. Thus, the results of EIS suggest that the discharge potential of Al-substituted α/β-nickel hydroxide should be higher

Table 2
Best fitting results of the Nyquist plots for the Al-substituted α/β-nickel hydroxide and the pure β-$Ni(OH)_2$ in high frequency region.

Electrode	R_L/Ω	R_{ct}/Ω	Y	n
α/β-Nickel hydroxide	0.41	0.88	0.024	0.71
Pure β-$Ni(OH)_2$	0.40	1.74	0.029	0.71

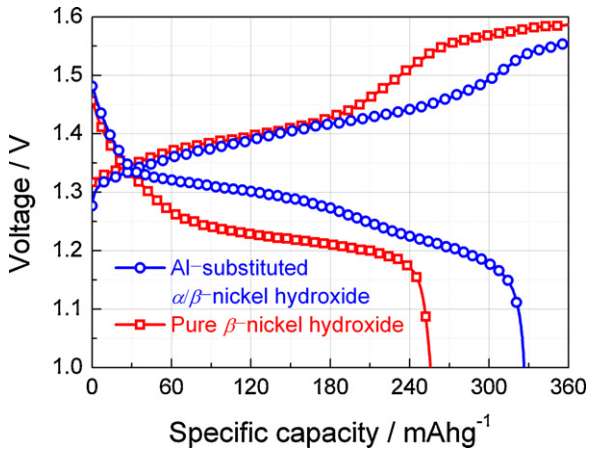

Fig. 8. Charge/discharge curves of pure β-Ni(OH)$_2$ and Al-substituted α/β-nickel hydroxide at the constant current density of 200 mA g^{-1}.

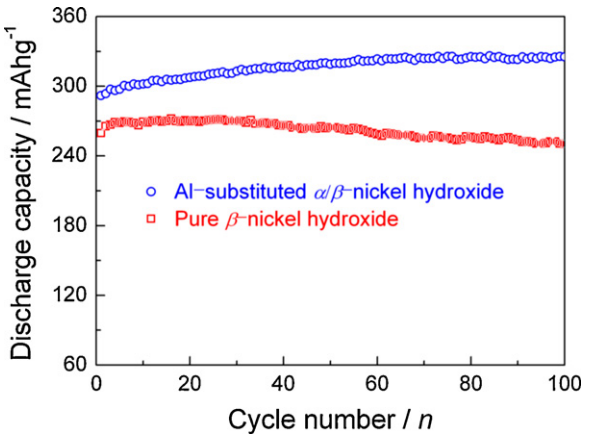

Fig. 9. Cyclic performance pure β-Ni(OH)$_2$ and Al-substituted α/β-nickel hydroxide at the charge/discharge current density of 200 mA g^{-1}.

than that of pure β-Ni(OH)$_2$, which can be further proved by the following charge/discharge test. In low frequency region, the Nyquist plots of both electrodes display a slope and the angle with the real axis is higher than 45°. This can be explained as a pseudo capacitive behavior, that is to say a close to linear vertical line, and as this behavior occurs in a porous nickel electrode, angle is reduced.

The lower charge-transfer resistance of Al-substituted α/β-nickel hydroxide can be attributed to the following reason. It is known that H^+ and OH^- move the fastest in aqueous solution because there is a proton relay system via hydrogen-bond network [40]. The α-nickel hydroxide within Al-substituted α/β-nickel hydroxide contains many water molecules and anions (see Figs. 2 and 5) throughout the interlayer space by the intermolecular hydrogen-bond network. This relay system is always in action in the process of oxidation and reduction, which facilitates the intercalation/de-intercalation of protons or the rapid movement of protons in the electrode. Therefore, smaller electrochemical reaction impedance can be obtained for the electrode with Al-substituted α/β-nickel hydroxide. However, for pure β-Ni(OH)$_2$, there is no such relay system due to the smaller interlayer space (about 4.6 Å as shown in Fig. 1). Therefore, the proton diffusion is greatly weakened and the electrochemical reaction impedance is increased in the electrode with pure β-Ni(OH)$_2$.

3.3. Charge/discharge test of the nickel electrode

Fig. 8 shows the typical charge/discharge curves of the two nickel electrodes at the constant current density of 200 mA g^{-1}. The specific discharge capacity of Al-substituted α/β-nickel hydroxide electrode is 326.6 mA h g^{-1}, which is 71.2 mA h g^{-1} higher than that (255.4 mA h g^{-1}) of pure β-Ni(OH)$_2$ electrode. The volumetric capacity of Al-substituted α/β-nickel hydroxide electrode is 659.7 mA h cm^{-3}. A single discharge plateau at about 1.22 V is observed for pure β-Ni(OH)$_2$ electrode. While Al-substituted α/β-nickel hydroxide electrode shows a much higher discharge plateau than pure β-Ni(OH)$_2$ electrode. In particular, two obvious discharge plateaus (at about 1.30 V and 1.22 V) are observed for Al-substituted α/β-nickel hydroxide electrode, indicating that two redox systems are involved in the electrochemical reactions. The scale of the individual discharge plateau is associated with the α-nickel hydroxide and β-nickel hydroxide in the mixture. The higher discharge plateau of Al-substituted α/β-nickel hydroxide electrode can be attributed to the larger quantity of water molecules within the interlayer space, which facilitate the proton diffusion during charge/discharge processes [41]. For the electrode with pure β-Ni(OH)$_2$, the charge curve presents two plateaus. The first plateau at about 1.39 V corresponds to the oxidation of β-Ni(OH)$_2$ to β-NiOOH, while the second plateau at about 1.57 V corresponds to the oxygen evolution reaction. For the electrode with Al-substituted α/β-nickel hydroxide, the charge curve shows three plateaus though the first plateau is not obvious. The first plateau at about 1.39 V and the second plateau at about 1.44 V are associated with β-nickel hydroxide and α-nickel hydroxide in the mixture, respectively. The third plateau at about 1.55 V is due to the oxygen evolution reaction.

The cyclic performance of the two electrodes at the constant current density of 200 mA g^{-1} is shown in Fig. 9. During the cycle processes, the electrode with Al-substituted α/β-nickel hydroxide shows much higher specific discharge capacity and better cycling stability than the electrode with pure β-Ni(OH)$_2$. The specific discharge capacity of the electrode with pure β-Ni(OH)$_2$ can be maintained to be about 270.0 mA h g^{-1} for the first 33 cycles, which reduces gradually in the following cycles and only 250.3 mA h g^{-1} can be obtained after 100 cycles. While for the electrode with Al-substituted α/β-nickel hydroxide, the specific discharge capacity increases gradually for the first 56 cycles, and can be maintained to be 325.4 mA h g^{-1} (or 657.3 mA h cm^{-3}) after 100 cycles. This indicates that the electrode with Al-substituted α/β-nickel hydroxide has much higher specific discharge capacity and better cyclic stability than the electrode with pure β-Ni(OH)$_2$.

The higher discharge capacity and better cyclic stability of Al-substituted α/β-nickel hydroxide arise due to its unique structure. The α/β mutually embedded structure combines the advantages of both α-nickel hydroxide and β-nickel hydroxide. The α-nickel hydroxide within Al-substituted α/β-nickel hydroxide has a higher specific discharge capacity and provides relay system for the proton diffusion in the electrode. Thus, the solid-state diffusion and intercalation/de-intercalation processes are remarkably improved, leading to a higher electrochemical activity. The β-nickel hydroxide in the two-phase mixture decreases the intimate interaction between the α-nickel hydroxide and the surrounding electrolyte and therefore improves the phase stability of α-nickel hydroxide in alkaline electrolyte. In addition, the relatively low substituted Al content in the α/β-nickel hydroxide may also increase the specific discharge capacity since Al is inefficient in the electrochemical redox reaction.

4. Conclusions

Al-substituted mixed phase α/β-nickel hydroxide was synthesized by a chemical coprecipitation method. It is found that the Al-substituted α/β-nickel hydroxide has a tap density of

2.02 g cm^{-3}, which is significantly higher than that of α-nickel hydroxide. Compared with pure β-Ni(OH)$_2$, the Al-substituted α/β-nickel hydroxide has higher electrochemical activity, better electrochemical reversibility, lower electrochemical resistance, and higher discharge voltage. Two discharge plateaus are observed for the Al-substituted α/β-nickel hydroxide due to the two phases of the nickel hydroxide. The specific discharge capacity of the Al-substituted α/β-nickel hydroxide maintains 325.4 mA h g^{-1} (or 657.3 mA h cm^{-3}) after 100 cycles at a charging–discharging current density of 200 mA g^{-1} at ambient temperature, which indicates that it may be a promising positive active material for alkaline secondary batteries. The relationship between the microstructure and the electrochemical performance of the Al-substituted α/β-nickel hydroxide was also discussed. The results reported in this work could be useful for the design and synthesis of nickel hydroxide materials with superior performance.

Acknowledgements

The authors thank the financial supports from the Guangxi Natural Science Foundation of China (Nos. 0991247, 0991004), Natural Science Foundation of China (50862002), Guangxi Science Research and Technology Developing Foundation of China (No. 0842003-15/16), and Guangxi Education Bureau Foundation of China (No. 200802LX191).

References

[1] A.K. Shukla, S. Venugopalan, B. Hariprakash, J. Power Sources 100 (2001) 125–148.
[2] A. Van der Ven, D. Morgan, Y.S. Meng, G. Ceder, J. Electrochem. Soc. 153 (2006) A210–A215.
[3] J.G. Wu, J.P. Tu, X.L. Wang, W.K. Zhang, Int. J. Hydrogen Energy 32 (2007) 606–610.
[4] W.K. Zhang, X.H. Xia, H. Huang, Y.P. Gan, J.B. Wu, J.P. Tu, J. Power Sources 184 (2008) 646–651.
[5] W. Zhang, W. Jiang, L. Yu, Z. Fu, W. Xia, M. Yang, Int. J. Hydrogen Energy 34 (2009) 473–480.
[6] A. Sierczynska, K. Lota, G. Lotaa, J. Power Sources 195 (2010) 7511–7516.
[7] M. Aghazadeh, A.N. Golikand, M. Ghaemi, Int. J. Hydrogen Energy 36 (2011) 8674–8679.
[8] D. Singh, J. Electrochem. Soc. 145 (1998) 116–120.
[9] R. Barnard, C.F. Randell, F.L. Tye, J. Appl. Electrochem. 10 (1980) 109–125.
[10] Y.W. Li, J.H. Yao, C.J. Liu, W.M. Zhao, W.X. Deng, S.K. Zhong, Int. J. Hydrogen Energy 35 (2010) 2539–2545.
[11] C. Faure, C. Delmas, P. Willmann, J. Power Sources 35 (1991) 263–277.
[12] L. Demourgues-Guerlou, C. Delmas, J. Power Sources 45 (1993) 281–289.
[13] L. Guerlou-Demourgues, C. Delmas, J. Electrochem. Soc. 143 (1996) 561–566.
[14] H. Chen, J.M. Wang, T. Pan, H.M. Xiao, J.Q. Zhang, C.N. Cao, Int. J. Hydrogen Energy 27 (2002) 489–496.
[15] L.J. Yang, X.P. Gao, Q.D. Wu, H.Y. Zhu, G.L. Pan, J. Phys. Chem. C 111 (2007), 4614-1619.
[16] T.A. Han, J.P. Tu, J.B. Wu, Y. Li, Y.F. Yuan, J. Electrochem. Soc. 153 (2006) A738–A742.
[17] Z. Liu, H. Zhen, Y. Kim, C. Liang, J. Power Sources 196 (2011) 10201–10206.
[18] Y.L. Zhao, J.M. Wang, H. Chen, T. Pan, J.Q. Zhang, C.N. Cao, Int. J. Hydrogen Energy 29 (2004) 889–896.
[19] M. Jayalakshmi, N. Venugopal, B. Ramachandra Reddy, M. Mohan Rao, J. Power Sources 150 (2005) 272–275.
[20] S. Nathira Begum, V.S. Muralidharan, C. Ahmed Basha, Int. J. Hydrogen Energy 34 (2009) 1548–1555.
[21] C. Nethravathi, N. Ravishankar, C. Shivakumara, M. Rajamathi, J. Power Sources 172 (2007) 970–974.
[22] P. Xu, X.J. Han, B. Zhang, Z.S. Lv, X.R. Liu, J. Alloys Compd. 436 (2007) 369–374.
[23] T.N. Ramesh, P. Vishnu Kamath, J. Power Sources 156 (2006) 655–661.
[24] H. Zhang, H. Liu, X. Cao, S. Li, C. Sun, Mater. Chem. Phys. 79 (2003) 37–42.
[25] P. Oliva, J. Leonardi, J.F. Laurent, C. Delmas, J.J. Braconnier, M. Figlarz, F. Fievet, A. de Guibert, J. Power Sources 8 (1982) 229–255.
[26] M. Hu, Z. Yang, L. Lei, Y. Sun, J. Power Sources 196 (2011) 1569–1577.
[27] Y.L. Zhao, J.M. Wang, H. Chen, T. Pan, J.Q. Zhang, C.N. Cao, Electrochim. Acta 50 (2004) 91–98.
[28] T. Pan, J.M. Wang, Y.L. Zhao, H. Chen, H.M. Xiao, J.Q. Zhang, Mater. Chem. Phys. 78 (2003) 711–718.
[29] J. Fan, Y. Yang, P. Yu, W. Chen, H. Shao, J. Power Sources 171 (2007) 981–989.
[30] Q.S. Song, C.H. Chiu, S.L.I. Chan, J. Solid State Electrochem. 12 (2008) 133–141.
[31] E. Shangguan, Z. Chang, H. Tang, X. Yuan, H. Wang, Int. J. Hydrogen Energy 35 (2010) 9716–9724.
[32] E. Shangguan, Z. Chang, H. Tang, X. Yuan, H. Wang, J. Power Sources 196 (2011) 7797–7805.
[33] W.-K. Hu, X.-P. Gao, D. Noreus, T. Burchardt, N.K. Nakstad, J. Power Sources 160 (2006) 704–710.
[34] J. Qi, P. Xu, Z. Lv, X. Liu, A. Wen, J. Alloys Compd. 462 (2008) 164–169.
[35] L. Wang, Z. Lu, F. Li, X. Duan, Ind. Eng. Chem. Res. 47 (2008) 7211–7218.
[36] F.-Y. Cheng, J. Chen, P.-W. Shen, J. Power Sources 150 (2005) 255–260.
[37] G.A. Snook, N.W. Duffy, A.G. Pandolfo, J. Power Sources 168 (2007) 513–521.
[38] D.A. Corrigan, R.M. Bendert, J. Electrochem. Soc. 136 (1989) 723–728.
[39] B. Liu, H. Yuan, Y. Zhang, Int. J. Hydrogen Energy 29 (2004) 453–458.
[40] P. Atkins, J.D. Paula, Physical Chemistry, 7th ed., Oxford University Press, Oxford, 2002.
[41] W.K. Hu, D. Noreus, Chem. Mater. 15 (2003) 974–978.